Structure of the growth interface of Y-Ba-Cu-O analogs on $SrTiO_3$ (001) substrates

M. Nakanishi and H. Hashizume*
Research Laboratory of Engineering Materials, Tokyo Institute of Technology, Nagatsuta, Midori, Yokohama 227, Japan

T. Terashima and Y. Bando
Institute for Chemical Research, Kyoto University, Uji 611, Japan

O. Michikami, S. Maeyama, and M. Oshima
NTT Interdisciplinary Research Laboratory, Tokai, Ibaraki 319-11 and Musashino, Tokyo 180, Japan
(Received 3 May 1993; revised manuscript received 21 June 1993)

The interface structures of *c*-axis-oriented ultrathin Gd-Ba-Cu-O and Eu-Ba-Cu-O films on $SrTiO_3$ (001) substrates have been determined using x-ray standing waves. Rare-earth fluorescence profiles observed near the 001 Bragg condition of $SrTiO_3$ show a dip without a marked peak, which can only be explained by either a BaO layer interfacing the TiO_2 plane of $SrTiO_3$ or the CuO or CuO_2 layer interfacing the SrO plane. Calculations of x-ray field intensities using a simple rigid-sphere-ion model show that for both Gd-Ba-Cu-O and Eu-Ba-Cu-O neither the CuO layer nor the CuO_2 layer can be the first grown layer on the TiO_2 surface of $SrTiO_3$. Similarly, neither the BaO layer nor the rare-earth layer can be the first layer on the SrO surface.

I. INTRODUCTION

Current interest in the device application of high-T_c thin-film superconductors is focused on heterostructures of Y-Ba-Cu-O (YBCO) on perovskite-type substrates. Widely used are $SrTiO_3$ (001) substrates, on which epitaxial YBCO crystals grow with the *a*, *b*, or *c* axis normal to the surface. The quality of thin-film crystals depends on the atomic structure at the growth interface, which is influenced by the substrate structure. Cubic $SrTiO_3$ has a lattice constant of $a=3.905$ Å, which is closely matched to $a=3.8591$, $b=3.9195$, and one-third of $c=11.8431$ Å of bulk $YBa_2Cu_3O_{7-x}$ at 623 °C.[1] The surface layer of $SrTiO_3$ (001) can be one of a SrO layer or a TiO_2 layer. The structural and chemical properties of these layers are similar to those of the *M*-O layer and the *M'*-O_2 layer present in the crystal structure of $YBa_2Cu_3O_{7-x}$, where *M* and *M'* are metals. These explain, even partly, why $SrTiO_3$ (001) is used for the growth of high-quality YBCO films.

Angle-resolved photoelectron-spectroscopy measurements indicate a TiO_2 plane for the surface layer terminating a $SrTiO_3$ (001) crystal.[2,3] Combining this information with high-resolution transmission-electron microscopy (HRTEM) images, Daitoh *et al.* proposed a model indicating a BaO layer of YBCO facing a substrate TiO_2 plane at the interface of a *c*-axis-oriented YBCO film on $SrTiO_3$ (001) (Ref. 4). This model was questioned by another HRTEM study which claimed that the near-interface lattice images were better explained by a CuO_2 layer of YBCO on a substrate SrO plane.[5] The issue concerns the interpretation of image contrasts at the heteroepitaxial interfaces, which is only qualitative. Actually, the two models become identical if the interface CuO_2 layer in the latter model is identified not as a first overlayer, but as a topmost TiO_2 plane of $SrTiO_3$.

We present here x-ray standing-wave (XSW) studies of the interface structure of Eu-Ba-Cu-O (EuBCO) and Gd-Ba-Cu-O (GdBCO) grown on $SrTiO_3$ (001) substrates. These compounds are analogs of YBCO with Eu or Gd atoms occupying the Y positions in the layered crystal structure of $YBa_2Cu_3O_{7-x}$. For the both materials, ultrathin superconducting films can be prepared on $SrTiO_3$ substrates using the techniques previously described.[6,7] The XSW method can determine the location of specific atoms above the substrate surface in the direction of the reciprocal-lattice vector, with reference to substrate lattice.[8–10] This is done by monitoring secondary emissions in the form of x-ray fluorescence or other radiations from overlayer atoms. At a synchrotron source, soft x-rays can be used to generate standing waves which excite the core levels of high-*Z* atoms that are convenient for measurement of fluorescent x-rays. Another advantage of soft x rays is a broad diffraction width, which relaxes the requirement for a high-crystalline perfection in the standing-wave producing substrate crystal.[11,12]

II. EXPERIMENTAL DETAILS

Ten layers of EuBCO were grown on the (001) surface of $SrTiO_3$ at 600 °C in a magnetron sputtering facility using a stoichiometric oxide target. The deposition rate was 38 Å/min in an Ar+8% O_2 atmosphere at 7 Pa. The previous work shows that the epitaxial crystal has the YBCO structure with the *c* axis normal to the surface.[6] GdBCO thin films were grown by depositing Gd, Ba, and Cu metals from individual evaporation sources onto $SrTiO_3$ (001) substrates at 680 °C in an oxygen atmosphere of 1 Pa.[7] Two and ten layers of GdBCO were grown on separate substrates at a deposition rate of 30 Å/min. The overlayer thickness was controlled by moni-

toring the reflection high-energy electron diffraction (RHEED) intensity oscillation. For both EuBCO and GdBCO, an N-layer-thick film denotes a film including N complete units of the YBCO structure in the surface normal direction.

X-ray measurements were performed on beamline 1A of the Photon Factory, a synchrotron radiation facility in Tsukuba, Japan. Beamline 1A provided soft x-ray photons of variable energy from a double InSb (111) monochromator. A sample was mounted on a vacuum diffractometer.[13] We generated an XSW field with an intensity modulation along the normal to the sample surface by exciting the 001 Bragg reflection of $SrTiO_3$ with 2.0 keV photons. The photon energy was so chosen that it produced electron holes in the M shells of Eu and Gd atoms, and the L shell of Sr atoms as well. This allowed us to measure 1.13-keV Eu $M\alpha$ and 1.19-keV Gd $M\alpha$ fluorescences from the EuBCO and GdBCO films, respectively, and a 1.81-keV Sr $L\alpha$ emission from the $SrTiO_3$ substrate. The energy resolution of a Si(Li) detector resolved the films and substrate emissions. The detector was placed outside the vacuum chamber at a 90° scattering angle in the horizontal plane, which contributed to a reduced background. A typical net count rate integrated over the energy range of the rare-earth line was 7/s for the ten-layer-thick GdBCO sample. The Bragg-reflected flux at $2\theta_B = 105.1°$ was monitored with the use of a photocurrent flowing through an in-vacuum metal grid.[14] Data were collected by scanning the sample θ angle for the fixed incoming photon energy.

III. RESULTS AND DISCUSSION

Eu fluorescence signals from the EuBCO sample were noisy, but θ-scan profiles showed a broad, shallow dip at the $SrTiO_3$ Bragg peak position. The data were normalized with the use of the flux monitor outputs, but the base line inclination was not removed from both the rocking curve and the emission profiles for reasons unknown.

Less noisy signals on a somewhat inclined base line were observed from ten-layer-thick GdBCO sample (Fig. 1). Gd M fluorescence yields show an asymmetric dip of ~ 0.26 in signal modulation at $\theta < \theta_B$, while the substrate 001 Bragg peak is located at $\theta = \theta_B$. The near-Gaussian profile of the rocking curve has a 580-μrad full width at half maximum, which is dominated by the instrument resolution. The dip in the Sr emission profile at $\theta \sim \theta_B$ is due to the extinction effect in the bulk $SrTiO_3$ crystal.[15]

To determine the atomic structure at the film-substrate interface, we calculate the XSW field intensity at the rare-earth atom (R) position in a model c-axis-oriented epitaxial RBCO film with one of the CuO(1), BaO(2), CuO_2(3), R(4), CuO_2(5), and BaO(6) layers on the substrate top layer atom plane. Both the TiO_2 plane and the SrO plane are considered for the $SrTiO_3$ (001) surface. The substrate atom planes are assumed to be planar, but for RBCO we employ the z coordinates of individual metals and oxygens for the YBCO crystal.[1] The two distinct O heights in the CuO_2 layer are averaged. Our calculation is based on a simple rigid-sphere-ion model. We use Pauling's ionic radii, but modify the Ti^{2+}, O^{2-}, and Cu

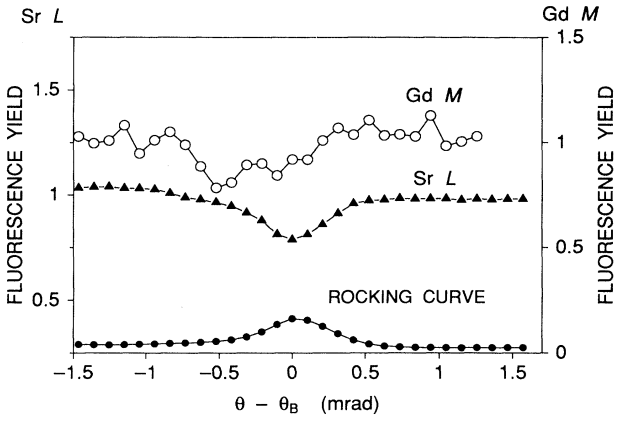

FIG. 1. Gd M fluorescence yields observed from a ten-layer-thick GdBCO film on a $SrTiO_3$ (001) substrate near the 001 Bragg peak of $SrTiO_3$ with incident 2.0 keV x rays. The average x-ray counts for 300 s are 2100 for the Gd M line and 210 000 for the Sr L line. The rocking curve is on an arbitrary scale. The synchrotron light source was injected with a 300 mA positron beam at 2.5 GeV.

radii so that the TiO_2, CuO, and CuO_2 square lattices have an edge length consistent with the lattice constant of $SrTiO_3$ (3.905 Å). This leads to $r(\mathrm{Ti}) = 0.638$ and $r(\mathrm{O}) = 1.314$ Å for the TiO_2 plane, $r(\mathrm{Cu}) = 0.794$ and $r(\mathrm{O}) = 1.158$ Å for the CuO and CuO_2 layers. Other ionic radii used are $r(O^{2-}) = 1.40$, $r(Sr^{2+}) = 1.13$, $r(Ba^{2+}) = 1.35$, $r(Eu^{3+}) = 1.03$, and $r(Gd^{3+}) = 1.02$ Å (Ref. 16). The vertical distance of the RBCO crystal from the substrate $SrTiO_3$ is determined on the assumption of contacting and noninterpenetrating ions at the interface. This distance depends on the atomic configurations in the interface planes and their relative position. On the TiO_2 plane, for example, the CuO_2 layer can take three positions with the Cu ions lying on top of the Ti, O, and face-centered positions of the TiO_2 square lattice. Other positions are not favored due to symmetry considerations. Geometry reveals that for the first and last positions, the interplanar distance d_P is determined by the O-O contact, while the Cu-O contact determines d_P for the second position, although the O-O contact would be unfavorable when we consider the electronic interaction. Table I summarizes the results of such investigations for the six distinct atom layers of GdBCO on the TiO_2 plane. In general, an on-top anion contact leads to a larger d_P than a cation-anion contact. An ion in a high-symmetry position can touch more than one underlying ions simultaneously.

Once d_P is calculated, it is easy to evaluate the vertical distance, d_1, of the first Gd layer from the interface TiO_2 plane. We employ 11.746 Å for the c-axis length of the GdBCO film,[17] and assume no lattice relaxation in the film and the substrate for the first approximation. The sixth column of Table I lists the normalized height $h_1 (= d_1/d_{001})$ of the first Gd plane, where d_{001} is the (001) lattice spacing of $SrTiO_3$. Note that the majority of h_1 values fall into two groups which are near integer and

TABLE I. Vertical positions of the Gd layer above a TiO_2 surface, calculated from a rigid-ion contact model. Ten layers of GdBCO lie above the $SrTiO_3$ (001) surface with either a CuO(1), BaO(2), CuO_2(3), Gd(4), CuO_2(5), or BaO(6) layer as the first layer. d_P is the interplanar distance at the film-substrate interface, d_1 and h_1 are the height of the first Gd layer and its normalized value, and z_{Gd} is the mean Gd height in a ten-layer-thick GdBCO film. See Fig. 2(a) for the definition of the distances.

No.	First layer	Contact ions	d_P (Å)	d_1 (Å)	h_1	z_{Gd}
1	CuO(1)	Cu-O	2.108	7.981	2.044	0.193
2	CuO(1)	O-O	2.472	8.345	2.137	0.286
3	BaO(2)	O-Ti	2.038	6.052	1.550	0.699
4	BaO(2)	Ba-Ti	1.988	5.697	1.459	0.608
5	BaO(2)	O-O	2.714	6.728	1.723	0.872
6	CuO_2(3)	Cu-O	2.108	3.803	0.974	0.123
7	CuO_2(3)	O-O	2.472	3.898	0.998	0.147
8	Gd(4)	Gd-O	2.334	2.334	0.598	0.747
9	Gd(4)	Gd-O_4	1.279	1.279	0.328	0.477
10	Gd(4)	Gd-Ti	1.658	1.658	0.425	0.574
11	CuO_2(5)	Cu-O	2.108	12.159	3.114	0.263
12	CuO_2(5)	O-O	2.472	12.792	3.276	0.425
13	BaO(6)	O-Ti	2.038	9.771	2.502	0.651
14	BaO(6)	Ba-Ti	1.988	10.026	2.568	0.717
15	BaO(6)	O-O	2.714	10.446	2.675	0.824

near half-integer. This arises from the interatomic distances at the interface similar to those in the $SrTiO_3$ crystal, and the fact that the c-axis length of the overlayer is only slightly mismatched to an integral multiple of d_{001}.

X-ray field intensity at an atom plane depends on the phase of the standing wave on that plane. The XSW phase is easily calculated using the concept of Bragg planes. The Bragg planes are located at the peaks in the Fourier component of the electron-density distribution. In the case of $SrTiO_3$ of ideal perovskite structure, the 001 component peaks between the TiO_2 planes and the SrO planes. If we take the unit-cell origin on a TiO_2 plane, for example, the 001 peaks are displaced from the TiO_2 planes by $[\eta_h/(2\pi)]d_{001}$, where η_h is the phase of the complex crystal structure factor $F_h = F_{hr} + iF_{hi} = |F_h|\exp(i\eta_h)$. It can be shown that the XSW phase at the chosen origin is $-\eta_h$ (Ref. 18). Clearly, the Bragg plane location, and hence the standing-wave phase, is independent of the origin definition for structure factor calculation. For the 001 reflection of $SrTiO_3$ with 2.0 keV x rays, $\eta_h/(2\pi) = -0.113$ with the origin on a TiO_2 plane. This large inward shift of the Bragg planes from the TiO_2 planes is due to the high-absorption factor of the Sr atoms at this energy, which makes F_{hi} negative while F_{hr} is positive.[19] A further complication with the lattice-mismatched system is that each Gd atom plane in an N-layer GdBCO film is excited by a slightly different phase of the 001 standing wave. This leads to a shift of the mean position, z_{Gd}, of the N Gd atom planes from h_1 by $(3/2)(N-1)[(d_{OL}/d_{001})-1]$, where d_{OL} is one-third the c-axis length of the overlayer GdBCO crystal.[18] The shift only amounts to 0.036 for $N=10$ in the present case. The mean position of the Gd planes with respect to the Bragg planes is thus given by

$$z_{Gd} = h_1 - \eta_h/(2\pi) + (3/2)(N-1)[(d_{OL}/d_{001})-1] .$$

The XSW phase at this position is $2\pi z_{Gd}$. The calculated z_{Gd} values are listed in the last column of Table I for the TiO_2 interface plane. Figure 2 depicts various distances in units of d_{001}. Similar results are obtained for GdBCO on the SrO plane of $SrTiO_3$ (Table II). It should be noted here that h_1 denotes the normalized height of the first Gd atom plane above the SrO plane, and that if we keep the unit-cell origin on a TiO_2 plane, an additional 0.5 should be added to the right-hand side of the above formula to give z_{Gd} for the SrO interface [cf. Fig. 2(b)]. In these tables arbitrary integer values were subtracted from z_{Gd} so that $0 \le z_{Gd} < 1.0$. Such subtractions correspond to shifting the XSW phase by $2n\pi$, and have no effect on the local-field intensity.

Figure 3 shows the Gd fluorescence profiles for hypothetical ten-layer-thick GdBCO films on $SrTiO_3$ (001) with Gd layers occupying mean positions $z_{Gd} = 0.0$ to 0.8 without disorder, calculated using formulae in Ref. 18. The curves take into account a 556-μrad angular divergence assumed for primary 2.0 keV x rays. Figure 3 also shows a rocking curve which is a convolution of the intrinsic curve with the Gaussian smearing function. The rocking curve shows a quite low peak reflectivity of 0.069, which is primarily due to the high absorption of the soft x rays in $SrTiO_3$. A direct consequence of this is a moderate intensity modulation of the standing-wave field, which is reflected in the fluorescence profiles. It is seen that $0.6 < z_{Gd} < 0.8$ produces an emission profile with an asymmetric dip at $\theta < \theta_B$ without a marked peak. With this kept in mind, an examination of Table I reveals that only BaO(2), Gd(4), and BaO(6) layers on the substrate TiO_2 plane can explain the observed Gd fluorescence profile. Similarly, Table II for the SrO interface shows that z_{Gd} values in the 0.6–0.8 range are only associated with the CuO(1), CuO_2(3), and CuO_2(5) layers at the interface.

TABLE II. Same as Table I but for a SrO plane at the $SrTiO_3$ (001) surface. See Fig. 2(b) for the definition of the distances.

No.	First layer	Contact ions	d_P (Å)	d_1 (Å)	h_1	z_{Gd}
1	CuO(1)	Cu-O	2.108	7.981	2.044	0.693
2	CuO(1)	O-O	2.472	8.345	2.137	0.786
3	CuO(1)	Cu-Sr	1.924	7.979	1.997	0.646
4	BaO(2)	Ba-O	2.664	6.372	1.632	0.281
5	BaO(2)	$O-O_2$	1.885	5.899	1.511	0.160
6	BaO(2)	O-O	2.714	6.728	1.723	0.372
7	CuO_2(3)	Cu-O	2.108	3.803	0.974	0.623
8	CuO_2(3)	O-O	2.472	3.898	0.998	0.647
9	CuO_2(3)	Cu-Sr	1.924	3.619	0.927	0.576
10	Gd(4)	Gd-O	2.334	2.334	0.598	0.247
11	Gd(4)	$Gd-O_2$	1.279	1.279	0.328	0.977
12	Gd(4)	Gd-Sr	2.150	2.150	0.551	0.200
13	CuO_2(5)	Cu-O	2.108	12.159	3.114	0.763
14	CuO_2(5)	O-O	2.472	12.792	3.276	0.925
15	CuO_2(5)	Cu-Sr	1.924	11.975	3.067	0.716
16	BaO(6)	Ba-O	2.664	10.702	2.741	0.390
17	BaO(6)	$O-O_2$	1.885	9.618	2.463	0.112
18	BaO(6)	O-O	2.714	10.446	2.675	0.324

The Gd layer may be removed from the list of the probable interface layers, since HRTEM pictures of ultrathin YBCO films on $SrTiO_3$ (001) show lattice images with very strong contrasts in the interface region, which are usually not ascribed to an Y layer, known to exhibit a much weaker contrast.[4]

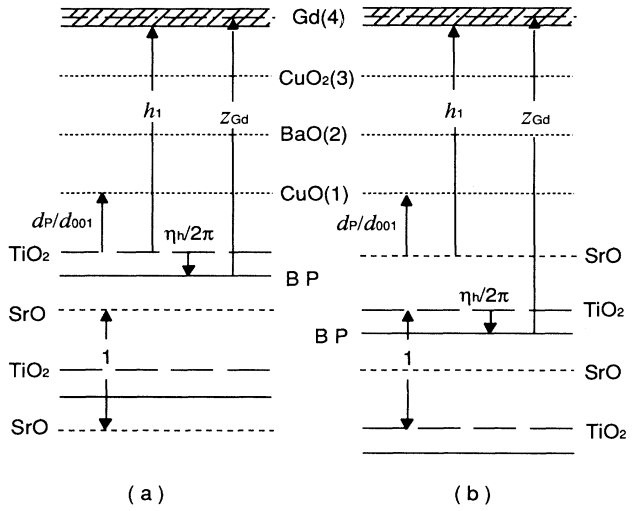

FIG. 2. Schematic diagrams showing various distances at the GdBCO/$SrTiO_3$ (001) interface for models with the TiO_2 plane (a) and the SrO plane (b) for the substrate top layer. d_P is the distance between the substrate's topmost atom plane and the first atom plane in GdBCO. h_1 is the height of the first Gd plane in GdBCO above the substrate top layer. The range of the distributed Gd planes due to the film-substrate lattice mismatch is shown by a shaded band. z_{Gd} defines the distance between the mean Gd atom plane position in a GdBCO thin film and the topmost (001) Bragg plane (BP) in $SrTiO_3$. $\eta_h/2\pi$ indicates the displacement of the Bragg planes from the TiO_2 planes on which the origin is placed for the structure factor calculation. All distances are illustrated in the units of d_{001}, the (001) lattice spacing of $SrTiO_3$. Drawn for a negative η_h.

Figure 4 shows the calculated Gd fluorescence profiles for ten-layer-thick, perfectly ordered GdBCO films with z_{Gd} values at 0.651, 0.699, and 0.717 for the BaO(6)/TiO_2 and BaO(2)/TiO_2 interfaces (cf. Table I). These curves include the effect of the distributed Gd positions around z_{Gd} due to the lattice mismatch[18] (cf. Fig. 2), although the effect is quite small, only reducing the overall coherent fraction by 1%. This indicates that our XSW measurement was well conditioned.[18] The experimental fluorescence profile in Fig. 4 was shifted toward the $+\theta$ direction by 233 μrad, even though we have no legitimate explanation for such a shift. A constant offset in the digital memory is a conceivable origin of the artifact. There is reasonable agreement between the experimental and calculated profiles, indicating the validity of our model. The scattered data do not allow us, however, to judge

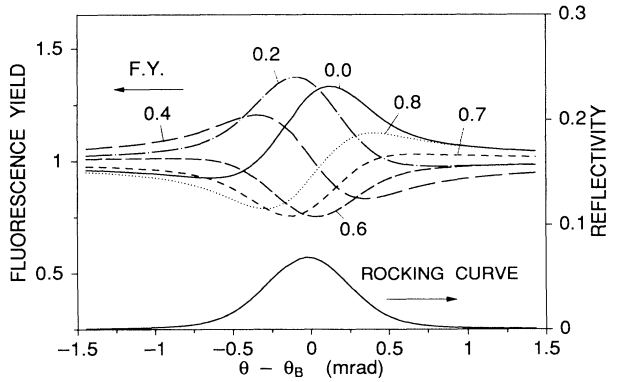

FIG. 3. Calculated fluorescence yield (F.Y.) profiles and rocking curve for ten-layer-thick GdBCO film on $SrTiO_3$ in the 001 reflection with 2.0-keV x rays. The F.Y. curves are calculated for the Gd atom planes occupying positions 0.0, 0.2, 0.4, 0.6, 0.7, and 0.8 between the (001) Bragg planes of $SrTiO_3$. All curves are convoluted with a Gaussian function of 556 μrad width.

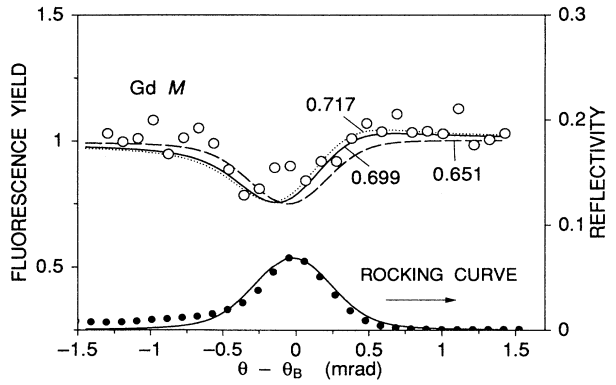

FIG. 4. Calculated emission yield profiles (line) for Gd atom planes at $z_{Gd}=0.651$, 0.699, and 0.717 (see Table I) compared with data (open circles). The observed rocking curve (closed circles) is fitted to the calculation at the peak and base levels.

which of the three curves shown best fits the data. Nevertheless, the large gaps in the z_{Gd} value between the first BaO-layer models and the first CuO- or CuO_2-layer models in Table I clearly reject the CuO layer and the CuO_2 layers for the interface layer of GdBCO on the TiO_2 plane. It is very likely that a BaO layer is the first grown layer on the substrate TiO_2 surface. A similar line of discussion leads to a conclusion that on the SrO surface of $SrTiO_3$, a CuO layer or a CuO_2 layer is the likely first epitaxial layer.

The almost equal ionic radii of Gd^{3+} and Eu^{3+} suggest that the above conclusions also apply to the EuBCO film. The ionic radius of Y^{3+} is ~ 0.1 Å smaller than $r(Gd^{3+})$ and $r(Eu^{3+})$ (Ref. 16). This will change the z_{Gd} values in Tables I and II by 0.025 to give the z_Y values for YBCO. These small changes would be far from changing the conclusions if we observe a dipped Y fluorescence profile from an YBCO film. The experiment is not easy to perform, however, since Y and Sr are too close in the periodic table for a current semiconductor detector to resolve the fluorescent x rays from the two atom species. This explains why we studied EuBCO and GdBCO films on a $SrTiO_3$ substrate.

It appears quite possible to discriminate between the models with the TiO_2 plane and the SrO plane at the growth interface, provided high-quality XSW data are available. Such data would also provide information on the registration of overlayer atoms with respect to the substrate atoms in the direction parallel to the interface, as well as on disorder in the high-T_c thin films.

IV. SUMMARY

Using soft x-ray standing waves, we have determined the interface structure of *c*-axis-oriented ultrathin GdBCO and EuBCO films on $SrTiO_3$ (001) substrates. Rare-earth fluorescence profiles observed near the 001 Bragg peak of $SrTiO_3$ show a dip without a marked peak, which can only be explained by either a BaO layer interfacing the TiO_2 plane or a CuO or CuO_2 layer interfacing the SrO plane of substrate $SrTiO_3$. Model calculations of x-ray field intensities based on contacting and noninterpenetrating ions at the interface show that neither the CuO layer nor the CuO_2 layer can be the first epitaxial layer on the TiO_2 surface of $SrTiO_3$. Similarly, neither the BaO layer nor the rare-earth layer can be the first grown layer on the SrO surface. The quality of our present data does not permit discriminating between the models assuming the TiO_2 plane and the SrO plane for the substrate surface, but it does show highly ordered Gd atoms in a ten-layer-thick GdBCO film.

ACKNOWLEDGMENTS

We are thankful to S. Brennan for the anomalous dispersion factors of Sr atoms and M. Sugiyama for assistance with experiments. This work was supported by the Photon Factory under Proposal No. 91-129.

*To whom all correspondence should be addressed.

[1]J. D. Jorgensen, M. A. Beno, D. G. Hinks, L. Soderholm, K. J. Volin, R. L. Hitterman, J. D. Grace, and I. K. Schuller, Phys. Rev. B **36**, 3608 (1987).

[2]M. Kawai, S. Watanabe, and T. Hanada, J. Cryst. Growth. **112**, 745 (1991).

[3]N. Terada, S. Yamamoto, S. Ishibashi, M. Jo, M. Hirabayashi, and H. Ihara, in *Advances in Superconductivity V,* Proceedings of the 5th International Symposium on Superconductivity (ISS'92), 1992, Kobe, edited by Y. Bando and H. Yamauchi (Springer-Verlag, Berlin, 1993), pp. 937–940.

[4]Y. Daitoh, K. Shimura, T. Terashima, and Y. Bando (unpublished).

[5]R. Ramesh, A. Inam, D. M. Hwang, T. S. Ravi, T. Sanda, X. X. Xi, X. D. Wu, Q. Li, T. Venkatesan, and R. Kilaas, J. Mater. Res. **6**, 2264 (1991).

[6]H. Asano, M. Asahi, and O. Michikami, Jpn. J. Appl. Phys. **89**, L981 (1989).

[7]T. Terashima, Y. Bando, K. Iijima, K. Yamamoto, K. Hirata, K. Hayashi, K. Kamigaki, and H. Terauchi, Phys. Rev. Lett. **65**, 2684 (1990).

[8]B. W. Batterman, Phys. Rev. **133**, A759 (1964).

[9]B. W. Batterman, Phys. Rev. Lett. **22**, 703 (1969).

[10]P. L. Cowan, J. A. Golovchenko, and M. F. Robbins, Phys. Rev. Lett. **44**, 1680 (1980).

[11]H. Hashizume and T. Nakahata, Jpn. J. Appl. Phys. **27**, L1568 (1988).

[12]M. Sugiyama, S. Maeyama, M. Oshima, H. Oigawa, Y. Nannichi, and H. Hashizume, Appl. Phys. Lett. **60**, 3247 (1992).

[13]S. Maeyama, K. Kawamura, and M. Oshima, Rev. Sci. Instrum. **62**, 2976 (1991).

[14]T. Nakahata, H. Hashizume, M. Oshima, and T. Kawamura, Jpn. J. Appl. Phys. **28**, L1300 (1989).

[15]J. R. Patel and J. A. Golovchenko, Phys. Rev. Lett. **50**, 1858 (1983).

[16]L. Pauling, *The Nature of the Chemical Bond,* 3rd ed. (Cornell

University Press, Ithaca, NY, 1960).
[17]E. E. Fullerton, J. Guimpel, O. Nakamura, and I. Schuller, Phys. Rev. Lett. **69**, 2859 (1992).
[18]Y. Saitoh, H. Hashizume, and K. Tsutsui, Jpn. J. Appl. Phys. **27**, 1386 (1988).

[19]F_{hr} and F_{hi} are defined as the parts of a crystal structure factor calculated from the real and imaginary parts of atomic scattering factors, respectively. Both quantities are real when the unit-cell origin is located at a center of symmetry.